Article

Developmental Cell

Environmental Oxygen Exposure Allows for the Evolution of Interdigital Cell Death in Limb Patterning

Graphical Abstract

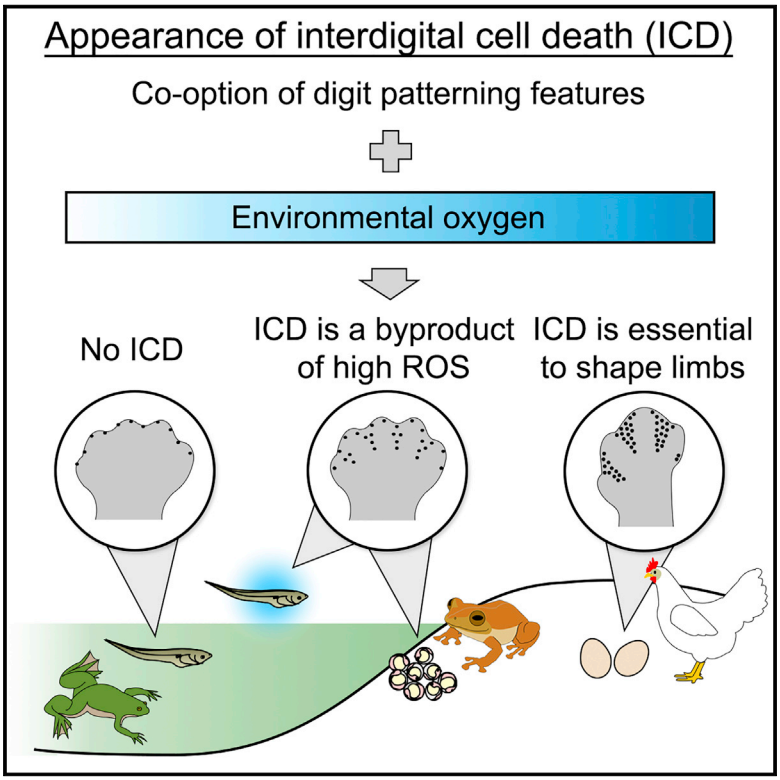

Highlights

- Interdigital cell death (ICD) is correlated with life-history strategy in tetrapods
- Atmospheric oxygen modulates local oxygen tension in the interdigital region
- High oxygen levels can induce ICD in an amphibian that typically lacks it
- Blood vessel density and Bmp signaling are critical for the appearance of ICD

Authors

Ingrid Rosenburg Cordeiro, Kaori Kabashima, Haruki Ochi, ..., Mara Laslo, James Hanken, Mikiko Tanaka

Correspondence

mitanaka@bio.titech.ac.jp

In Brief

Interdigital cell death (ICD) correlates with life-history strategy in tetrapods, occurring in amniotes, but not in amphibians. Cordeiro et al. show that atmospheric oxygen regulates ICD by modulating blood vessel density and Bmp signaling. Increasing oxygen levels induces ICD in an amphibian that typically lacks it.

Cordeiro et al., 2019, Developmental Cell *50*, 1–12
July 22, 2019
https://doi.org/10.1016/j.devcel.2019.05.025

CellPress

Please cite this article in press as: Cordeiro et al., Environmental Oxygen Exposure Allows for the Evolution of Interdigital Cell Death in Limb Patterning, Developmental Cell (2019), https://doi.org/10.1016/j.devcel.2019.05.025

Developmental Cell
Article

Environmental Oxygen Exposure Allows for the Evolution of Interdigital Cell Death in Limb Patterning

Ingrid Rosenburg Cordeiro,[1] Kaori Kabashima,[1] Haruki Ochi,[2] Keijiro Munakata,[1] Chika Nishimori,[1] Mara Laslo,[3] James Hanken,[3] and Mikiko Tanaka[1,4,*]
[1]School of Life Science and Technology, Tokyo Institute of Technology, B-17, 4259 Nagatsuta-cho, Midori-ku, Yokohama 226-8501, Japan
[2]Institute for Promotion of Medical Science Research, Faculty of Medicine, Yamagata University, 2-2-2 Iida-Nishi, Yamagata, Yamagata 990-9585, Japan
[3]Department of Organismic and Evolutionary Biology and Museum of Comparative Zoology, Harvard University, 26 Oxford Street, Cambridge, MA 02138, USA
[4]Lead Contact
*Correspondence: mitanaka@bio.titech.ac.jp
https://doi.org/10.1016/j.devcel.2019.05.025

SUMMARY

Amphibians form fingers without webbing by differential growth between digital and interdigital regions. Amniotes, however, employ interdigital cell death (ICD), an additional mechanism that contributes to a greater variation of limb shapes. Here, we investigate the role of environmental oxygen in the evolution of ICD in tetrapods. While cell death is restricted to the limb margin in amphibians with aquatic tadpoles, *Eleutherodactylus coqui*, a frog with terrestrial-direct-developing eggs, has cell death in the interdigital region. Chicken requires sufficient oxygen and reactive oxygen species to induce cell death, with the oxygen tension profile itself being distinct between the limbs of chicken and *Xenopus laevis* frogs. Notably, increasing blood vessel density in *X. laevis* limbs, as well as incubating tadpoles under high oxygen levels, induces ICD. We propose that the oxygen available to terrestrial eggs was an ecological feature crucial for the evolution of ICD, made possible by conserved autopod-patterning mechanisms.

INTRODUCTION

The shape of the autopods—hands and feet—has a critical role in the adaptation of tetrapods to their habitats. Amphibians form digits free of interdigital webbing through differential proliferation of digital and interdigital cells (Cameron and Fallon, 1977; Vlaskalin et al., 2004). Amniotes, however, also require cell death during limb development, an additional layer of regulation that contributes to the formation of species-specific features (Cooper et al., 2014; Fallon and Cameron, 1977; Fernández-Terán et al., 2006; Salas-Vidal et al., 2001), including unique morphologies such as the coot leg (*Fulica atra*; Zuzarte-Luis and Hurle, 2005) and the bat wing (*Carollia perspicillata*; Weatherbee et al., 2006). Interdigital cell death (ICD) has not been observed in amphibians (Cameron and Fallon, 1977; Vlaskalin et al., 2004), except in one salamander species (Franssen et al., 2005); factors responsible for the acquisition of this new process by amniotes are still unknown.

Bmp signaling is required for triggering programmed cell death in the limb (Kaltcheva et al., 2016; Yokouchi et al., 1996; Zou and Niswander, 1996; Zuzarte-Luis and Hurle, 2005), although the underlying mechanism is still unclear. In addition, sufficient levels of reactive oxygen species (ROS) are independently required for this process (Eshkar-Oren et al., 2015; Salas-Vidal et al., 1998; Schnabel et al., 2006). Environmental oxygen levels can modulate ROS levels in a tissue-specific way, regulating both developmental processes and adult homeostasis (Covarrubias et al., 2008; Puente et al., 2014; Wagenfuhr et al., 2015). In this context, one innovation of amniotes in relation to amphibians comes to mind: the amniote egg, whose evolution was critical for the invasion of the terrestrial environment by providing the developing embryo with high oxygen levels while avoiding dehydration (Berner et al., 2007; Schmidt-Nielsen, 1997). Could environmental differences during the development of amniotes and amphibians regulate local oxygen levels in the limb, affecting ROS production and the incidence of cell death?

Here, we explore the origins of ICD by using experimental approaches and multispecies comparisons to determine how ecological changes may have contributed directly to the evolution of vertebrate limb shape after the water-to-land transition.

RESULTS

Bmp Signaling Does Not Explain Differences in ICD between *X. laevis* and Amniotes

Cell death is observed throughout the chicken's interdigital region (Figure 1A), but it is restricted to the limb margin in the African clawed frog, *Xenopus laevis* (Figure 1C), as labeled by LysoTracker-positive cells (white arrows in Figures 1B′ and 1D′). This stain identifies the increased lysosomal activity observed in dying cells and phagocyted cell debris (Zuzarte-Luis et al., 2007; Boya and Kroemer, 2012; Fogel et al., 2012).

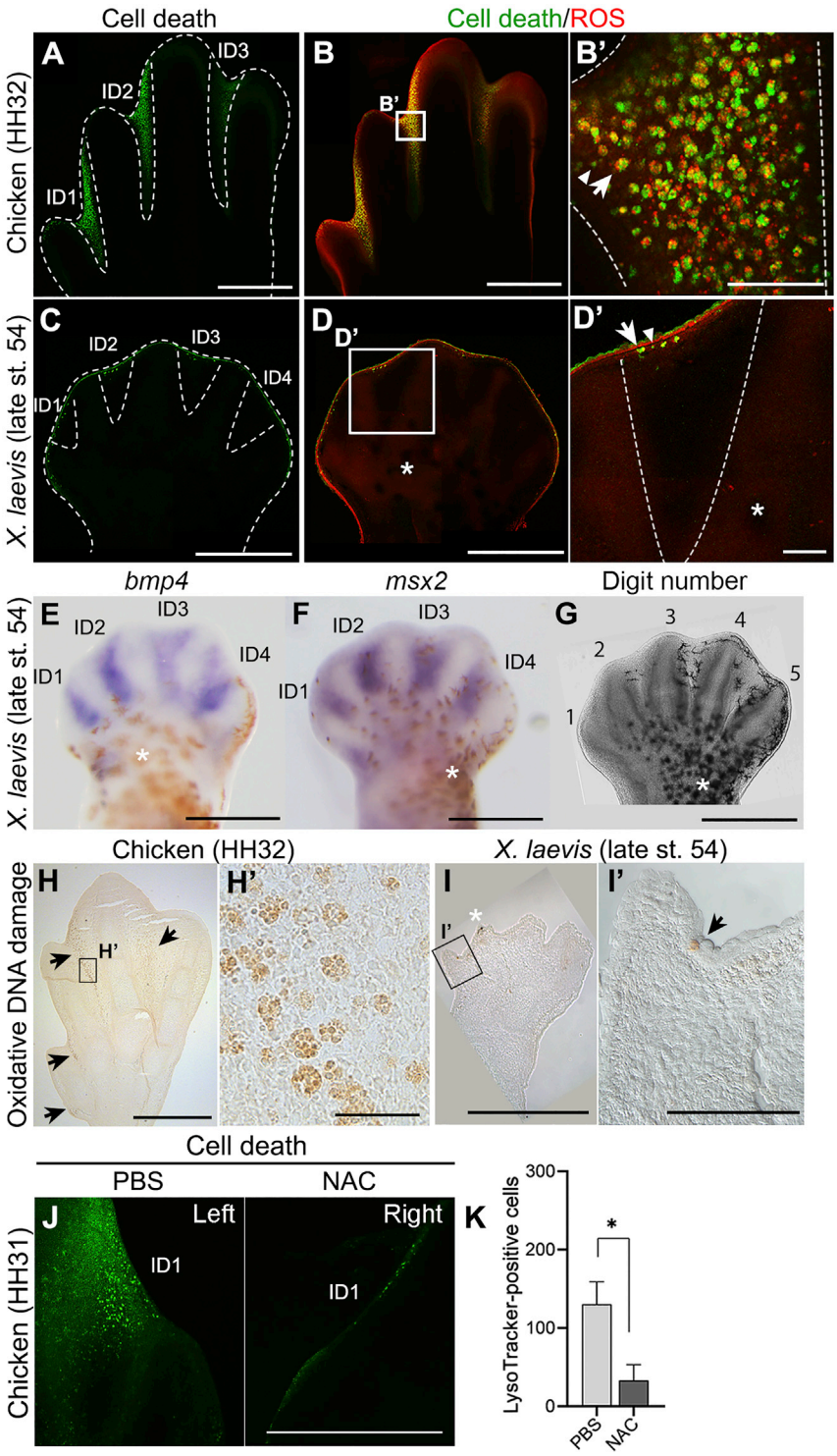

Figure 1. Correlation between Cell Death, ROS, and Oxidative DNA Damage in Tetrapod Limbs

(A–D) Cell death (LysoTracker green) and ROS (DHE) staining of HH32 chicken hindlimbs (n = 6) and late stage 54 *X. laevis* hindlimbs (n = 5). (A) and (C) Cell death is found throughout the interdigital region (dashed lines) of chicken, but not of *X. laevis*. (B) and (D) The same pattern is observed regarding ROS production. (B′) and (D′) Higher magnification of rectangles in (B) and (D). White arrows point to LysoTracker-positive cells; white arrowheads indicate lysosomal activity that may not be related to cell death (smaller LysoTracker puncta).

(E and F) Expression pattern of *bmp4* (n = 3) and *msx2* (n = 6) in late stage 54 *X. laevis* hindlimbs.

(G) Morphology of a late stage 54 *X. laevis* hindlimb (n = 11) revealing that all digit cartilages are already present (numbered as 1–5).

(H and I) Cells stained with 8-oxoguanine (black arrows) in HH32 chicken hindlimbs (n = 3) and late stage 54 *X. laevis* hindlimbs (n = 4).

(J) Cell death (LysoTracker green) in stage HH31 chicken forelimbs incubated for 6 h with the ROS scavenger N-acetyl-cysteine (NAC, right limbs; PBS, left limbs; n = 5).

(K) Quantification of LysoTracker-positive cells in the interdigit 1 (ID1) of limbs in (J). Mean ± SEM. Two-tailed paired t test.

Brown or black cells are pigment cells (white asterisks), not stained cells. ID1–4, interdigital regions 1–4. Scale bars, 1 mm (H), 500 μm (A–G, I , and J), 100 μm (B′ and D′), and 20 μm (H′ and I′). See also Figures S1 and S2.

In amniote autopods, Bmp signaling is required for regulating digit number prior to the induction of cell death (Chimal-Monroy et al., 2003; Fernández-Terán et al., 2006; Raspopovic et al., 2014). We hypothesized that cell-death-promoting Bmp signaling would be absent from the *X. laevis* interdigital region following its role in establishing digit number at stages 52–53 (Jones et al., 2013; Keenan and Beck, 2016). However, *bmp4* (Satoh et al., 2005) and its target gene *msx2* are expressed in interdigital regions during subsequent stages (Figures 1E–1G and S1A–S1C). Thus, we sought to identify which other factor was required for inducing cell death in the interdigital membrane of tetrapods.

Oxygen and ROS Regulate ICD in Tetrapod Limbs

As ROS are required for ICD in mice (Eshkar-Oren et al., 2015; Salas-Vidal et al., 1998; Schnabel et al., 2006), we considered whether they are decisive for ICD in other tetrapods. Chickens have extensive ROS production in the interdigital region (Figure 1B) as well as in other areas of cell death in the limb mesenchyme and the apical ectodermal ridge (AER) (Figures S2A–S2H). In *X. laevis*, high ROS production is restricted to LysoTracker-positive cells in the limb margin, but not in the interdigital region, at all observed stages (Figures 1D, S1D, and S1E). The same pattern is observed for cells containing the oxidative damage marker 8-oxoguanine (Figures 1H and 1I). Decreasing ROS levels by using N-acetyl-cysteine inhibits ICD in chicken

(Figures 1J and 1K), indicating that ROS are not only a by-product of cell death in the limb.

We next tested if atmospheric oxygen is a modulator of cell death in the limb by using a multigas incubator. Incubating chicken limbs under hypoxia is sufficient to inhibit cell death in the interdigital mesenchyme (Figures 2A and 2D) as well as the anterior necrotic zone of younger embryos (Figures 2B and 2E). Conversely, incubation under hyperoxia increases the number of LysoTracker-positive cells specifically in the interdigital region (Figures 2C and 2D). Given its inductive role in chicken limbs, we tested if increased environmental oxygen could promote cell death in the interdigital region of an amphibian, *X. laevis*. Hyperoxia provided an approximately 3-fold increase in the amount of dissolved oxygen in the water around the tadpoles (from 7.9 ± 0.7 ppm, SD, n = 5 to 22.2 ± 1.3 ppm, SD, n = 5). After 3 h, a patch of cell death appeared specifically across the interdigital region under hyperoxia, but not normoxia (Figures 2F and 2G). The LysoTracker-positive cells are in the mesenchyme (Figure 2G′). The ectopic ICD is detected at late stage 54 and stage 55 tadpoles, but not at other stages (Figures 2H and S1F–S1H), while the pattern of cell death in the tadpole body (Figures S3A and S3B) (such as in the olfactory organs; Dittrich et al., 2016) and forelimbs (Figures S3C–S3E) is unchanged. Cell death was accompanied by increased ROS production (Figures 2I and 2J), while neither the expression of the Bmp target gene *msx2* (Figure 2K) nor cell proliferation rates are affected by this treatment (Figures S3F–S3J). A mild reduction of the interdigital membranes can be observed in some of the limbs after one week of hyperoxia (Figures S3K–S3M). Thus, environmental oxygen levels directly affect ROS production within the limb, even promoting ICD in an amphibian that typically lacks it.

Blood Vessel Remodeling Is Correlated with Stages Permissive to Cell Death in Tetrapods

Besides atmospheric oxygen levels, blood vessels are also essential for tissue oxygenation. Blood vessel maturation by remodeling improves perfusion (Potente et al., 2011) and is correlated with the onset of ICD in mice (Eshkar-Oren et al., 2015). We considered whether the timing of blood remodeling is distinct between chicken and *X. laevis*.

Remodeling is first evident around the finger condensations in both chicken and *X. laevis* (Figures 3A and 3B, arrows). A hierarchically branched network forms in the interdigital region of chicken during ICD stages (Figure 3A, asterisks). Importantly, vascular remodeling also occurs in the *X. laevis* interdigital region during the stages when ICD can be induced by high oxygen levels (Figure 3B, asterisks). Remodeling progresses in a similar manner throughout limb development in both chicken and *X. laevis* and also coincides with active Bmp signaling (Figure 3). These data highlight how a common potential mechanism for the induction of ICD under sufficient oxygen levels may be shared among diverse tetrapods.

Increasing Limb Vasculature Density Promotes ICD in *X. laevis*

To test directly if blood vessel density can induce ICD in an amphibian, we generated transgenic *X. laevis* that overexpressed *VegfA-b*, a proangiogenic factor ortholog of the mammalian *VegfA*, under the control of the mouse limb-specific promoter *Prrx1* (Martin and Olson, 2000; Suzuki et al., 2007) (Figure 4A). Reporter expression is observed throughout the limb bud mesenchyme (Figures 4E and S4A). When compared to wild-type tadpoles, *Prrx1-VegfA-EGFP* tadpoles have increased blood vessel density in the limbs at early stage 54 (Figures 4B–4D). Increased ROS production is also observed at the same stage (Figure S4B). No difference in cell proliferation is observed between wild-type and transgenic hindlimbs (Figures S4C and S4D). Transgene expression decreases as tissues differentiate (Suzuki et al., 2007), and by stage 56 the vasculature is not significantly different from that in wild-type limbs (Figures S4E and S4F).

At late stage 54, reporter expression was stronger in the anterior region and absent in the distal portion of the foot plate in a wedge shape (Figure 4E), as observed in *Prx1-LacZ* transgenic mice (Martin and Olson, 2000). Notably, at this stage, all *Prrx1-VegfA-EGFP* tadpoles have ectopic patches of cell death specifically in the interdigital mesenchyme (Figures 4F and 4G). The ectopic cell death is detected in interdigital spaces 1 and 2 (Figure 4H), consistent with the stronger anterior expression of the transgene (Figure 4E, which is the same limb as Figure 4G). Cells with high ROS production are also observed in the same region (Figures 4I and 4J). Thus, increasing the density of blood vessels—the source of oxygen in the limbs—promotes cell death specifically in the interdigital mesenchyme of *X. laevis*.

The Correlation between ICD and Environmental Oxygen Levels Is Conserved in Other Amphibians

To add a comparative perspective, the distribution of cell death and ROS was assessed in two other amphibian species: the Japanese fire-bellied newt, *Cynops pyrrhogaster*, and the coquí frog, *Eleutherodactylus coqui*. In *C. pyrrhogaster*, sparse LysoTracker-positive cells are found around the growing digits (Vlaskalin et al., 2004), but not in the interdigital region in all investigated stages (Figures 5A and S5A); ROS production is also restricted to those cells (Figures 5B and S5B). Blood vessels in *C. pyrrhogaster* autopods are found only around the budding digits (Figures 5C and S5C) and do not extend into the interdigital region (Figure 5C). In contrast, cell death is detected in the interdigital region and limb margin of both forelimbs and hindlimbs of *E. coqui* (Figures 5D, S5D, and S5E). Both LysoTracker-positive and surrounding cells in the interdigital mesenchyme have increased ROS production (Figure 5E), as seen in chicken (Figure 1B). Blood vessels of *E. coqui* extend over a large area of the interdigital region (Figure 5F). We detected a small number of LysoTracker-positive cells at all times due to their large cell size in relation to overall limb size (Figure 5E), a pattern similar to that reported in the seepage salamander, *Desmognathus aeneus*, the only other amphibian species in which ICD has been observed (Franssen et al., 2005).

There is an important ecological difference between these species at the stages when limbs are developing. Both *E. coqui* and *D. aeneus* have direct development: fertilized eggs are laid on land, and an immature adult animal emerges at the end of the embryonic period; there is no free-living, aquatic larval stage (Hanken et al., 2001). This life history is more comparable to that seen in amniotes than it is to the biphasic life history, which includes a discrete metamorphosis between aquatic larva and terrestrial adult, that is characteristic of *X. laevis*, *C. pyrrhogaster* (reported here), and all other amphibian species in which cell death has

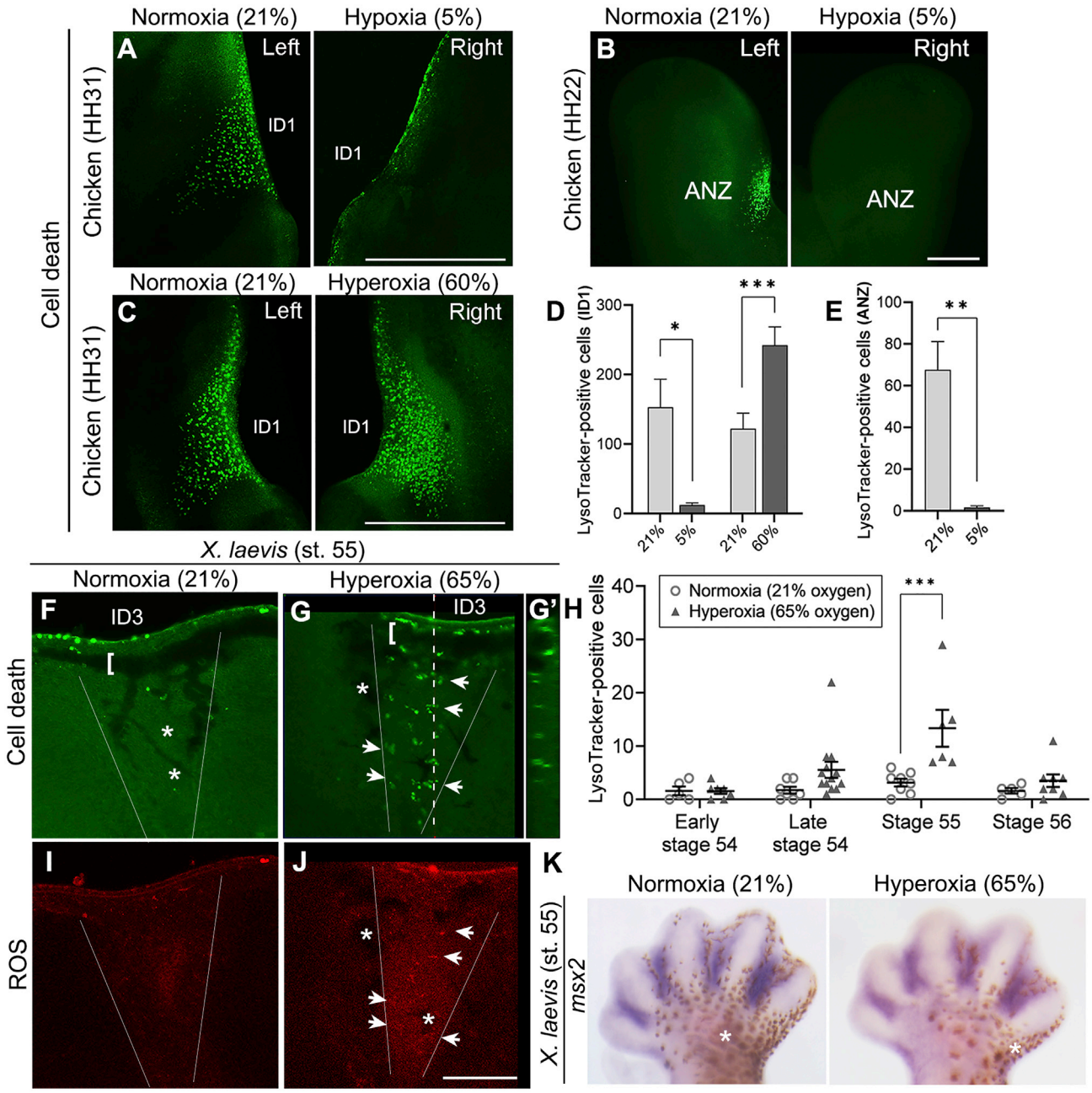

Figure 2. Atmospheric Oxygen Levels Regulate Interdigital Cell Death in Tetrapods

(A) Cell death (LysoTracker green) in stage HH31 chicken forelimbs incubated for 6 h under hypoxia (5% oxygen, right limbs; 21% oxygen, left limbs; n = 5). ID1, interdigital region 1.

(B) Cell death (LysoTracker green) in stage HH22 chicken forelimbs incubated for 6 h under hypoxia (5% oxygen, right limbs; 21% oxygen, left limbs; n = 6). ANZ, anterior necrotic zone.

(C) Cell death (LysoTracker green) in stage HH31 chicken forelimbs incubated for 6 h under hyperoxia (60% oxygen, right limbs; 21% oxygen, left limbs; n = 8).

(D) Quantification of LysoTracker-positive cells in the interdigit 1 (ID1) of limbs in (A) and (C). Mean ± SEM. Two-tailed paired t test.

(E) Quantification of LysoTracker-positive cells in the ANZ of limbs in (B). Mean ± SEM. Two-tailed paired t test.

(F, G, I, and J) Cell death (LysoTracker green; F and G) in stage 55 *X. laevis* hindlimbs incubated under normoxia (n = 8) or hyperoxia (n = 6). ID3, interdigital region 3. Ectopic cell death is observed in the interdigital region proximal to the marginal vein (white brackets) and in the mesenchyme, as revealed by the orthogonal section in (G′). ROS staining (CellROX Deep red; [I] and [J]) of the same limbs under normoxia (n = 4) or hyperoxia (n = 5) revealed LysoTracker-positive cells with increased ROS levels (white arrows).

(legend continued on next page)

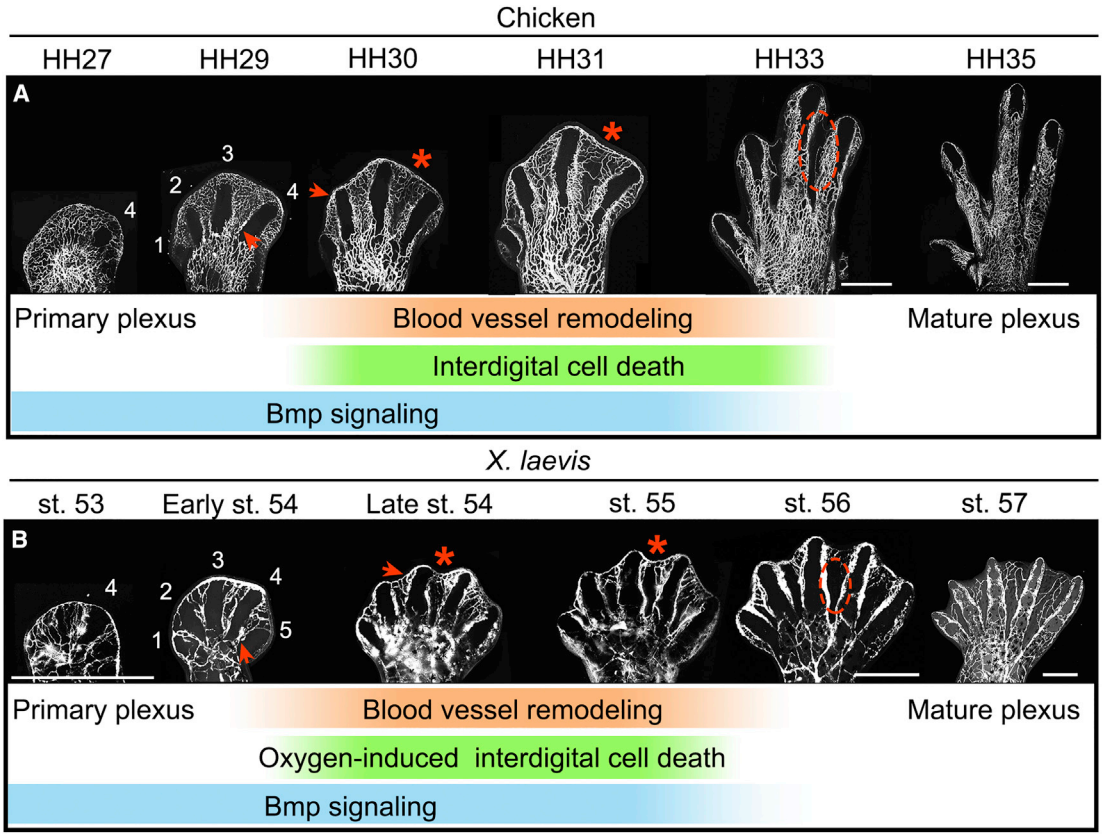

Figure 3. Blood Vessel Remodeling Is Correlated with Stages Permissive to Cell Death in Tetrapods

(A and B) Vasculature (fluorescent ink injection) of chicken hindlimbs (HH27, n = 4; HH29, n = 3; HH30, n = 9; HH31, n = 8; HH32, n = 4; HH33, n = 4; HH35, n = 3) and *X. laevis* hindlimbs (stage 53, n = 6; early stage 54, n = 5; late stage 54, n = 3; stage 55, n = 3; stage 56, n = 4; stage 57, n = 5). Vascular remodeling induced by the newly formed finger cartilages is observed firstly in the perichondral region (red arrows) and then in the interdigital region (red asterisk) of both species. During remodeling stages, interdigital cell death is observed or can be experimentally induced in chicken and *X. laevis*, respectively; interdigital Bmp signaling is also still active (Figures S1A and S1B). At a later stage, regression of the vasculature is observed (red lines).

Images of the vasculature of chicken (HH29 and HH31) and *X. laevis* (early stage 54 and late stage 54) are also represented in Figures 3A and 3B. ID1–4, interdigital regions 1–4. Scale bars, 1 mm (A) and 500 μm (B).

been investigated, including *Ambystoma maculatum*, *Ambystoma mexicanum*, *Bufo americanus*, *Notophthalmus viridescens*, and *Taricha torosa* (Cameron and Fallon, 1977; Vlaskalin et al., 2004). As obtaining oxygen from the air is more efficient than from the water (Schmidt-Nielsen, 1997), differences in life history have an important consequence for limb development: limbs in metamorphosing species develop in aquatic environments whereas limbs in direct-developing species develop in terrestrial eggs, under atmospheric oxygen. Thus, high oxygen availability is correlated with the presence of cell death during limb development of tetrapods (Figure 5G).

The Oxygen Profile of the Limbs Is Distinct between Chicken and *X. laevis*

In light of the above results, we asked how the different oxygen levels surrounding the embryo or tadpole translated to a local, tissue level during limb development. We measured oxygen tension profiles of the tissues by using EF5, which binds to proteins only under hypoxia and is then recognized by ELK3 antibodies (Figure S6A) (Koch, 2002); ELK3 antibodies previously saturated with its ligand EF5 were used as a control, the "competed" stain (Figures S6B, S6D, and S6E) (Koch, 2002). We validated our methodology by measuring oxygen distribution in the chicken neural tube, which was high in the dorsal side (Figure S6C) as reported previously (Dias et al., 2014).

Chicken limbs have a high oxygen tension in the interdigital region (Figure 6A) with levels that reach the upper limit that this method can detect (at least 1% oxygen concentration in the tissue when no EF5 binding is found) (Koch, 2002). In contrast, the digits have lower oxygen levels (Figure 6A). This pattern is observed at all stages, beginning with the appearance of the interdigital

(H) Quantification of LysoTracker-positive cells in all interdigital regions in (F), (G), and Figures S1F– S1H. Mean ± SEM. Two-tailed unpaired t test.

(K) *msx2* expression pattern in stage 55 *X. laevis* hindlimbs under normoxia (n = 6) or hyperoxia (n = 8).

Brown or black cells are pigment cells (white asterisks), not stained cells. Scale bars, 500 μm (A–C) and 100 μm (F, G, I, and J). Significance was defined as $p \leq 0.05$ (*p < 0.05, **p < 0.01, ***p < 0.001). See also Figures S1 and S3.

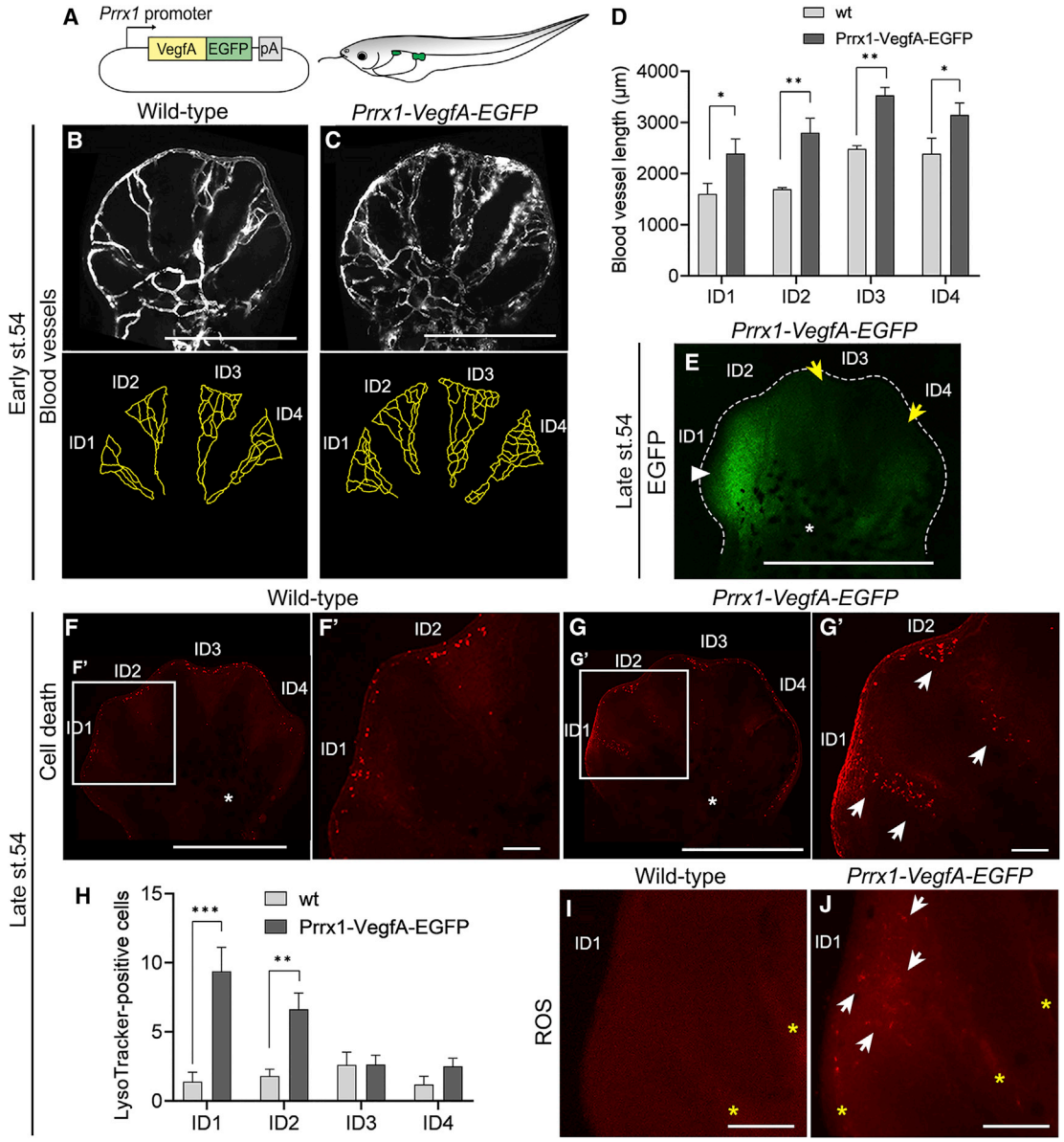

Figure 4. Blood Vessel Density Regulates ICD in Tetrapods

(A) Schematic diagram of the *Prrx1-VegfA-EGFP* expression plasmid and transgenic frog.

(B and C) Vasculature (fluorescent ink, upper panels) of early stage 54 wild-type (n = 5) and *Prrx1-VegfA-EGFP* hindlimbs (n = 6). Transgenic limbs have higher blood vessel density, as evidenced by manually tracing the blood vessels paths (bottom panels).

(D) Quantification of the length of the blood vessels of hindlimbs in (B) and (C) revealed increased blood vessel density in all interdigital regions by early stage 54. Mean ± SEM. Two-tailed unpaired t test.

(E) EGFP fluorescence in late stage 54 hindlimbs (n = 14) is more intense in the anterior region (white arrowhead). Reporter expression has disappeared from the middle portion of the autopod (yellow arrows), as reported in mice (Martin and Olson, 2000).

(F and G) Cell death (LysoTracker red) in wild-type (n = 5) and *Prrx1-VegfA-EGFP* (n = 8) hindlimbs at late stage 54. (F′) and (G′) Higher magnification of panels in (F) and (G). Transgenic limbs have ectopic cell death in the anterior region (white arrows).

(H) Quantification of LysoTracker-positive cells in each interdigital region of limbs in (F) and (G). Mean ± SEM. Two-tailed unpaired t test.

(I and J) ROS staining (CellROX Deep Red) of late stage 54 wild-type (n = 6) and *Prrx1-VegfA-EGFP* (n = 4) hindlimbs. Ectopic ROS production (white arrows) is detected in cells in the anterior region in transgenic limbs. Yellow asterisks, fixation artifact.

Brown or black cells are pigment cells (white asterisks), not stained cells. ID1–4, interdigital regions 1–4. Scale bars, 500 μm (B, C, E, F, and G) and 100 μm (F′, G′, I, and J). Significance was defined as $p \leq 0.05$ (*$p < 0.05$, **$p < 0.01$, ***$p < 0.001$). See also Figure S4.

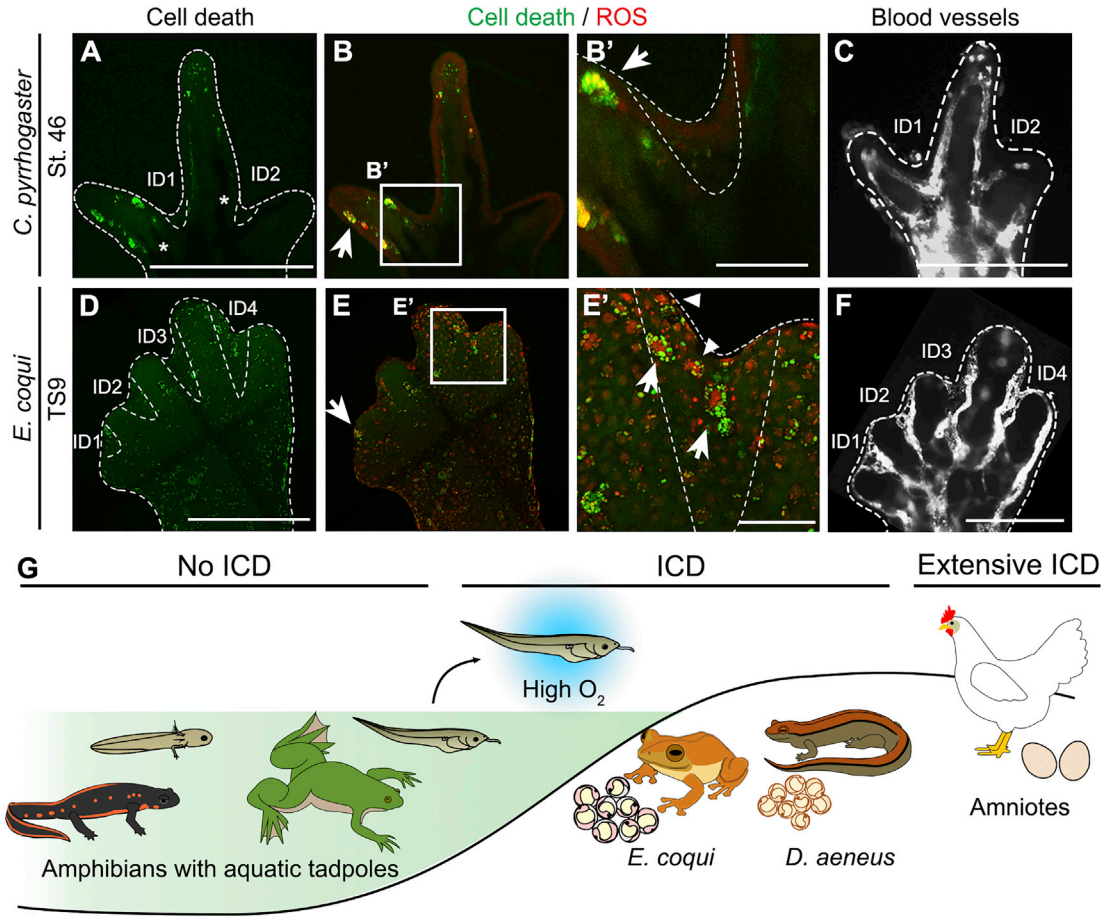

Figure 5. ICD and Environmental Oxygen Are Correlated in Various Tetrapods

(A, B, D, and E) Cell death (LysoTracker green) and ROS (DHE) staining in stage 47 *C. pyrrhogaster* forelimbs (n = 6) and TS9 *E. coqui* hindlimbs (n = 7). (A) and (C) Cell death is not found in the interdigital regions (dashed lines) of *C. pyrrhohaster*, but is found in *E. coqui*. (B) and (D) The same pattern is observed regarding ROS production. (B′) and (E′) Higher magnifications of the rectangles in (B) and (E). White arrows point to LysoTracker-positive cells. White arrowheads indicate ROS-producing cells containing only LysoTracker puncta.

(C and F) Vasculature (fluorescent ink injection) of *C. pyrrhogaster* forelimbs (stage 47, n = 5) and TS9 *E. coqui* hindlimbs (TS9, n = 5).

(G) Cartoon illustrating the life history and limb development strategies of investigated amphibians. *X. laevis*, *C. pyrrhogaster* (both reported here), and amphibians (Cameron and Fallon, 1977; Vlaskalin et al., 2004) have aquatic tadpoles and no ICD, while *E. coqui* (reported here) and *D. aeneus* (Franssen et al., 2005) lay terrestrial-direct-developing eggs and have ICD. Extensive ICD is observed in amniotes.

Black cells are pigment cells (white asterisks), not stained cells. ID1–4, interdigital regions 1–4. Scale bars, 500 μm (A–F) and 100 μm (B′ and E′). See also Figure S5.

regions (Figures 6B and S6F–S6J). Additionally, hypoxia is observed in the joints, in mesenchyme under the AER, and in phalanx-forming regions (Figures S6F–S6J).

Next, we investigated oxygen distribution in the limbs of *X. laevis*. It is not possible to directly compare fluorescence levels among species due to possible differences in the uptake of EF5, but one can compare the staining pattern. In a striking difference from chicken, the interdigital regions of *X. laevis* are hypoxic, even if mild hypoxia is also observed in the fingers (Figure 6C). Low oxygen tension is detected in the interdigital region as soon as the digit-interdigit pattern becomes evident at stage 52 and continues in subsequent stages (Figures 6D and S6K–S6P). Other landmarks of digit development, however, have an oxygen profile similar to that observed in chicken: the distal mesenchyme of the limb buds, the phalanx-forming region (PFR), and the joints are also hypoxic in *X. laevis* (Figures S6K–S6P). These data reveal that the oxygen tension profile of the interdigital region, but not of other limb structures, is distinct between chicken and *X. laevis*.

Finally, we evaluated if oxygen concentration in the tissue is responsive to environmental oxygen levels. Hypoxia, which inhibits cell death in chicken limbs (Figures 2E and 2G), reduces tissue oxygen tension specifically in the interdigital mesenchyme (Figures 6E–6G). On the other hand, incubating *X. laevis* under hyperoxia—a condition that induces ectopic ICD (Figures 2H–2J)—increases oxygen tension in the interdigital region (Figures 6H–6J). Thus, oxygen tension of the interdigital region, a highly vascularized tissue, is correlated with environmental oxygen levels that surround the embryo or tadpole.

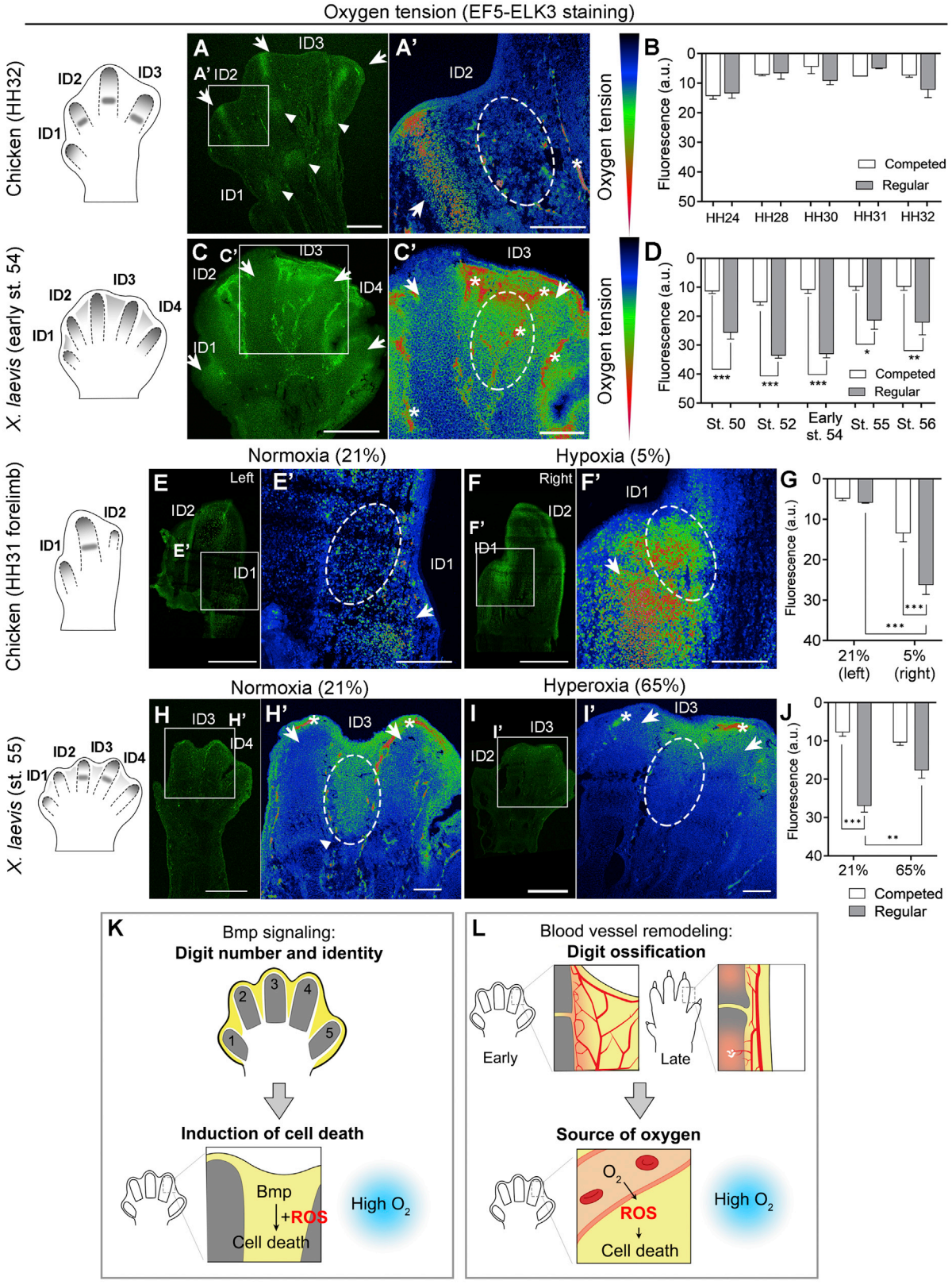

(legend on next page)

DISCUSSION

Features of Digit Patterning Make the Interdigital Region Permissive to Cell Death

Here, we propose that the life-history strategy regulates oxygen availability in the limbs, with high oxygen levels being necessary for the appearance of cell death in the interdigital region. One key aspect of this hypothesis is understanding why the amphibian interdigital region is permissive for the induction of cell death, even in species in which cell death does not normally occur. Bmp signaling and a blood-vessel-dependent source of oxygen are independently related to ICD in amniotes, as suggested by results of transgenic mouse studies (Eshkar-Oren et al., 2015; Kaltcheva et al., 2016) and those reported here (Figure 2K). Bmp signaling in the interdigital region is part of a self-regulatory network that patterns both digit periodicity and identity of tetrapods (Hiscock et al., 2017; Huang et al., 2016; Jones et al., 2013; Montero et al., 2008; Onimaru et al., 2016; Raspopovic et al., 2014; Suzuki et al., 2008). Bmps are also expressed in the interdigital region in the coquí frog (Gross et al., 2011) and the axolotl (Guimond et al., 2010). Inhibition of Bmps also causes generalized defects in chondrogenesis in both amniotes and amphibians (Chimal-Monroy et al., 2003; Jones et al., 2013), suggesting that finger patterning and skeletogenesis were at least part of the ancestral role of Bmps in the autopod prior to the appearance of ICD (Figure 6K).

Likewise, vascular patterning is a fundamental feature of skeletal morphogenesis, which is induced by signals from the emerging cartilages (Eshkar-Oren et al., 2009) that form a perichondral plexus required for ossification during later stages (Gerber et al., 1999; Zelzer et al., 2002). In the autopod, remodeling signals from the digit cartilages extend to the interdigital region and lead to areas of high local oxygen availability (Eshkar-Oren et al., 2015) (Figure 6L). It is fascinating to speculate that an independent developmental step, ICD, might have emerged from two preexisting traits of digit morphogenesis in the presence of increased environmental oxygen levels (Figures 6K and 6L).

Molecular Sensors of Oxygen and Their Possible Roles during Limb Development

Sensing and responding to variable oxygen levels is crucial for the homeostasis of aerobic organisms. Hypoxia-inducible factors (HIF) play several roles during development (Dunwoodie, 2009), including digit chondrogenesis, ossification, and joint formation (Amarilio et al., 2007; Mangiavini et al., 2014; Provot et al., 2007). In line with these reports, we also observed hypoxia in the developing fingers and joints of both chicken and *X. laevis* (Figures 6 and S6). On the other hand, the molecular responses to hyperoxia and ROS during development are not as well understood in a physiological context. ROS are required for cell death in chicken (this report) and mice limbs (Eshkar-Oren et al., 2015; Salas-Vidal et al., 1998), and in addition the expression of antioxidant enzymes decreases in the interdigital region of mice during ICD stages (Schnabel et al., 2006). The balance between production and elimination of ROS affects redox-sensitive proteins, directly influencing cell signaling (Covarrubias et al., 2008; Ray et al., 2012).

We previously identified the role of the redox-sensitive AP-1 transcription factors in regulating the balance between cell survival and death in chicken limbs (Suda et al., 2014). While MafB/c-Fos dimers and the antioxidant-response-associated Nrf-2 inhibited cell death, MafB/c-Jun dimers promoted cell death, with MafB being expressed specifically in the interdigital region under control of the Bmp pathway (Suda et al., 2014). c-Jun has also been shown to regulate cell death in younger chicken limb buds (Grotewold and Rüther, 2002). Additionally, the proapoptotic pathway p38, which can be directly activated by ROS (Ray et al., 2012), is active in the chicken interdigital region and is in part regulated by Bmps (Zuzarte-Luíz et al., 2004). Thus, it is possible that AP-1 transcription factors, among other redox-sensitive pathways, mediate the effect of hyperoxia in the interdigital regions. Given the complex role of the signaling pathways mentioned above in regulating cell survival and death, future studies will be required to understand the exact role microenvironmental oxygen levels have during limb development.

Figure 6. Oxygen Tension Profile in the Interdigital Region of Chicken and *X. laevis* Was Dependent on Atmospheric Oxygen Levels

The fluorescence of the EF5-ELK3 staining is inversely correlated with tissue oxygen tension, making it a hypoxia marker. Autofluorescent red blood cells were a fixation artifact found in all samples (white asterisks) and were not quantified.

(A and C) EF5-ELK3 staining of HH32 chicken hindlimbs (regular, n = 4) and early stage 54 *X. laevis* hindlimbs (regular, n = 4). Fingers (white arrows) and joints (white arrowheads) were hypoxic. (A′) and (C′) Higher magnifications of the rectangles in (A) and (C) are shown in pseudocolor. The interdigital regions (dashed lines) had higher oxygen levels in chicken than in frog. Cartoons to the left indicate hypoxic regions.

(B and D) Quantification of fluorescence intensity in the interdigital region of limbs in (A), (C), and Figures S6D–S6H and S6K–S6N reveals that the interdigital regions in *X. laevis*, but not chicken, are hypoxic. Mean ± SEM. Two-tailed unpaired t test.

(E and F) EF5-ELK3 staining of HH31 chicken limbs (regular, n = 7; competed, n = 5) incubated under hypoxia (right) or normoxia (left). (E′) and (F′) Higher magnifications of the rectangles in (E) and (F) are shown in pseudocolor. Hypoxia reduced the oxygen tension in the interdigital region (dashed lines). The cartoon represents hypoxic regions in untreated limbs.

(G) Quantification of fluorescence intensity in the interdigital region of (E) and (F). Mean ± SEM. Two-way ANOVA test.

(H and I) EF5-ELK3 staining of stage 55 *X. laevis* incubated under hyperoxia (regular, n = 13; competed, n = 6) or normoxia (regular, n = 8; competed, n = 4). (H′) and (I′) Higher magnifications of the rectangles in (H) and (I) are shown in pseudocolor. Hyperoxia increased the oxygen tension in the interdigital region (dashed lines). The cartoon represents hypoxic regions in untreated limbs.

(J) Quantification of fluorescence intensity in the interdigital region of (H) and (I). Mean ± SEM. Two-way ANOVA test.

(K and L) Model of the evolutionary history of ICD in tetrapods. (K) Interdigital Bmp signaling (yellow) is essential for the periodic patterning of digits and interdigits as well as establishing digit identity. In amniotes, Bmp is essential for ICD when sufficient ROS are available. (L) Early finger condensations induce the formation of a rich perichondral plexus that allows a timely vascular invasion of the ossification center and bone formation. In the autopod, the early remodeling process also increases interdigital blood vessel density, providing an abundant oxygen source linked to ROS production and ICD.

a.u., arbitrary units. ID1–4, interdigital regions 1–4. Scale bars, 500 μm (A, E, F, H, and I), 200 μm (A′, C, E′, and F′), and 100 μm (C′, H′, and I′). Significance was defined as $p \leq 0.05$ (*$p < 0.05$, **$p < 0.01$, ***$p < 0.001$). See also Figure S6.

Terrestrial Eggs Increased Oxygen Availability during Evolution

While all animals are adapted to obtain oxygen from their respective environments, the air's increased oxygen content and decreased mass in comparison to water makes air breathing more efficient (Schmidt-Nielsen, 1997); hyperoxia alone has a positive effect on vertebrate developmental rate and body size (Berner et al., 2007). However, increased environmental oxygen also has deleterious effects, such as loss of the heart regenerative potential in the mammalian heart as a consequence of the oxygen-rich postnatal environment (Puente et al., 2014). Balancing the positive and negative effects of ROS appears to have been a critical step in the invasion of oxygenated settings by animals as a whole, as ROS are regulators of cell proliferation, differentiation, and death (Covarrubias et al., 2008; Hammarlund et al., 2018). Consistent with this idea, we observed lower oxygen levels in the AER and phalanx-forming region (Figure S6), two highly proliferating tissues that regulate the extension of the limbs and fingers, respectively (Montero et al., 2008; Summerbell et al., 1973; Suzuki et al., 2008).

We propose that terrestrial-direct development is causally associated with increased oxygen availability and ICD in tetrapods, but it remains to be determined if cell death was initially only a by-product of increased ROS levels or a preexisting adaptive feature. For instance, tropical salamanders (*Bolitoglossa* spp.) evolved webbed feet multiple times, mostly as a consequence of the evolution of correlated traits and not as the primary targets of adaptation (Jaekel and Wake, 2007). The very mild reduction of the interdigital webbing in *X. laevis* incubated for one week under hyperoxia (Figures S3K–S3M) indicates that ICD may not yet be integrated to the limb patterning in amphibians. In the same way, whether cell death plays a role in limb morphogenesis of *E. coqui* (Figure 5) or *D. aeneus* (Franssen et al., 2005) is presently unknown. Hence, investigating additional direct-developing species (Wake and Hanken, 1996), as well as determining why the differential tissue growth employed by amphibians was insufficient to remove the interdigital region in amniotes (Cameron and Fallon, 1977; Salas-Vidal et al., 2001), will be essential to fully elucidate the origins of cell death as a novel step in the evolution of limb development in amniotes.

STAR★METHODS

Detailed methods are provided in the online version of this paper and include the following:

- KEY RESOURCES TABLE
- CONTACT FOR REAGENT AND RESOURCE SHARING
- EXPERIMENTAL MODEL AND SUBJECT DETAILS
- METHOD DETAILS
  - Probe Synthesis and In Situ Hybridization
  - Detection of Cell Death and Reactive Oxygen Species
  - Immunohistochemistry
  - Cell Proliferation Analysis
  - Visualization of Blood Vessels
  - Oxygen or NAC Incubation
  - Plasmid Construction and Generation of *X. laevis* Transgenics
  - Quantitative Measurement of Oxygen Tension in the Tissue
  - Images
- QUANTIFICATION AND STATISTICAL ANALYSIS
  - Quantification
  - Statistical analysis

SUPPLEMENTAL INFORMATION

Supplemental Information can be found online at https://doi.org/10.1016/j.devcel.2019.05.025.

ACKNOWLEDGMENTS

We thank Dr. Kimberly Cooper, Dr. Shigeru Kuratani, and Dr. Atsushi Kawakami for critical comments; Dr. Akihiro Watanabe for donating newt larvae; Dr. Makoto Suzuki, Dr. Bau-Lin Huang, Dr. Akira Satoh, Dr. Takashi Kato, and Dr. Daisuke Sakai for technical advice; Dr. Cameron J. Koch for providing EF5 reagent and ELK3 antibodies; Mr. Matthew Gage for technical support; the Harvard Center for Biological Imaging and Dr. Douglas Richardson for imaging support; and the Biotechnology Center of Tokyo Institute of Technology for sequencing services. This work was supported by a Grant-in-Aid for Scientific Research (B) (16H04828), a Grant-in-Aid for Scientific Research on Innovative Areas (18H04818), the Takeda Science Foundation, and the Fujiwara Natural History Foundation to M.T.; Grant-in-Aid for Scientific Research (C) (16K07362), (B) (17KT0049), the Takeda Science Foundation, and the Suzuken Memorial Foundation to H.O.; and the U.S. National Science Foundation number DEB-1701591 to J.H.; the transgenic vector (*ISXexEGFP*) was provided by the Institute for Amphibian Biology (Hiroshima University, Japan) with support in part by the National Bio-Resource Project of the Japan Agency for Medical Research and Development (AMED) under grant number JP18km0210085.

AUTHOR CONTRIBUTIONS

I.R.C., K.K., and M.T. designed the project. I.R.C. and M.T. wrote the manuscript. I.R.C. and K.K. performed the experiments except those described otherwise. H.O. generated transgenics and provided *X. laevis* tadpoles and related materials. K.K. and K.M. constructed plasmids. C.N. made blood vessel injections in chicken. M.L. supported *E. coqui* experiments. J.H. provided *E. coqui* embryos and infrastructure.

DECLARATION OF INTERESTS

The authors declare no competing interests.

Received: December 10, 2018
Revised: April 1, 2019
Accepted: May 10, 2019
Published: June 13, 2019

REFERENCES

Amarilio, R., Viukov, S.V., Sharir, A., Eshkar-Oren, I., Johnson, R.S., and Zelzer, E. (2007). HIF1 regulation of Sox9 is necessary to maintain differentiation of hypoxic prechondrogenic cells during early skeletogenesis. Development *134*, 3917–3928.

Berner, R.A., VandenBrooks, J.M., and Ward, P.D. (2007). Evolution. Oxygen and evolution. Science *316*, 557–558.

Boya, P., and Kroemer, G. (2008). Lysosomal membrane permeabilization in cell death. Oncogene *27*, 6434–6451.

Cameron, J.A., and Fallon, J.F. (1977). The absence of cell death during development of free digits in amphibians. Dev. Biol. *55*, 331–338.

Chimal-Monroy, J., Rodriguez-Leon, J., Montero, J.A., Gañan, Y., Macias, D., Merino, R., and Hurle, J.M. (2003). Analysis of the molecular cascade responsible for mesodermal limb chondrogenesis: sox genes and BMP signaling. Dev. Biol. *257*, 292–301.

Cooper, K.L., Sears, K.E., Uygur, A., Maier, J., Baczkowski, K.S., Brosnahan, M., Antczak, D., Skidmore, J.A., and Tabin, C.J. (2014). Patterning and post-patterning modes of evolutionary digit loss in mammals. Nature *511*, 41–45.

Covarrubias, L., Hernández-García, D., Schnabel, D., Salas-Vidal, E., and Castro-Obregón, S. (2008). Function of reactive oxygen species during animal development: passive or active? Dev. Biol. *320*, 1–11.

Dias, J.M., Ilkhanizadeh, S., Karaca, E., Duckworth, J.K., Lundin, V., Rosenfeld, M.G., Ericson, J., Hermanson, O., and Teixeira, A.I. (2014). CtBPs sense microenvironmental oxygen levels to regulate neural stem cell state. Cell Rep. *8*, 665–670.

Dittrich, K., Kuttler, J., Hassenklöver, T., and Manzini, I. (2016). Metamorphic remodeling of the olfactory organ of the African clawed frog, *Xenopus laevis*. J. Comp. Neurol. *524*, 986–998.

Dunwoodie, S.L. (2009). The role of hypoxia in development of the mammalian embryo. Dev. Cell *17*, 755–773.

Eshkar-Oren, I., Krief, S., Ferrara, N., Elliott, A.M., and Zelzer, E. (2015). Vascular patterning regulates interdigital cell death by a ROS-mediated mechanism. Development *142*, 672–680.

Eshkar-Oren, I., Viukov, S.V., Salameh, S., Krief, S., Oh, C.-d, Akiyama, H., Gerber, H.-P., Ferrara, N., and Zelzer, E. (2009). The forming limb skeleton serves as a signaling center for limb vasculature patterning via regulation of Vegf. Development *136*, 1263–1272.

Fallon, J.F., and Cameron, J. (1977). Interdigital cell death during limb development of the turtle and lizard with an interpretation of evolutionary significance. J. Embryol. Exp. Morphol. *40*, 285–289.

Fernández-Terán, M.A., Hinchliffe, J.R., and Ros, M.A. (2006). Birth and death of cells in limb development: a mapping study. Dev. Dyn. *235*, 2521–2537.

Fogel, J.L., Thein, T.Z.T., and Mariani, F.V. (2012). Use of LysoTracker to detect programmed cell death in embryos and differentiating embryonic stem cells. J. Vis. Exp. *68*, 4254.

Franssen, R.A., Marks, S., Wake, D., and Shubin, N. (2005). Limb chondrogenesis of the seepage salamander, *Desmognathus aeneus* (Amphibia: plethodontidae). J. Morphol. *265*, 87–101.

Gerber, H.P., Vu, T.H., Ryan, A.M., Kowalski, J., Werb, Z., and Ferrara, N. (1999). VEGF couples hypertrophic cartilage remodeling, ossification and angiogenesisduring endochondral bone formation. Nat. Med. *5*, 623–628.

Gross, J.B., Kerney, R., Hanken, J., and Tabin, C.J. (2011). Molecular anatomy of the developing limb in the coquí frog, *Eleutherodactylus coqui*. Evol. Dev. *13*, 415–426.

Grotewold, L., and Rüther, U. (2002). The Wnt antagonist Dickkopf-1 is regulated by Bmp signaling and c-Jun and modulates programmed cell death. EMBO J. *21*, 966–975.

Guimond, J.C., Lévesque, M., Michaud, P.L., Berdugo, J., Finnson, K., Philip, A., and Roy, S. (2010). BMP-2 functions independently of SHH signaling and triggers cell condensation and apoptosis in regenerating axolotl limbs. BMC Dev. Biol. *10*, 15.

Gurdon, J.B. (1995). Normal table of *Xenopus laevis* (Daudin). Trends Genet. *11*, 418.

Hamburger, V., and Hamilton, H.L. (1951). A series of normal stages in the development of the chick embryo. J. Morphol. *88*, 49–92.

Hammarlund, E.U., von Stedingk, K., and Påhlman, S. (2018). Refined control of cell stemness allowed animal evolution in the oxic realm. Nat. Ecol. Evol. *2*, 220–228.

Hanken, J., Carl, T.F., Richardson, M.K., Olsson, L., Schlosser, G., Osabutey, C.K., and Klymkowsky, M.W. (2001). Limb development in a "nonmodel" vertebrate, the direct-developing frog *Eleutherodactylus coqui*. J. Exp. Zool. *291*, 375–388.

Hiscock, T.W., Tschopp, P., and Tabin, C.J. (2017). On the formation of digits and joints during limb development. Dev. Cell *41*, 459–465.

Huang, B.-L.L., Trofka, A., Furusawa, A., Norrie, J.L., Rabinowitz, A.H., Vokes, S.A., Mark Taketo, M., Zakany, J., Mackem, S., Taketo, M.M., et al. (2016). An interdigit signalling centre instructs coordinate phalanx-joint formation governed by 5′Hoxd-Gli3 antagonism. Nat. Commun. *7*, 1–10.

Jaekel, M., and Wake, D.B. (2007). Developmental processes underlying the evolution of a derived foot morphology in salamanders. Proc. Natl. Acad. Sci. USA *104*, 20437–20442.

Jones, T.E.M., Day, R.C., and Beck, C.W. (2013). Attenuation of bone morphogenetic protein signaling during amphibian limb development results in the generation of stage-specific defects. J. Anat. *223*, 474–488.

Kaltcheva, M.M., Anderson, M.J., Harfe, B.D., and Lewandoski, M. (2016). BMPs are direct triggers of interdigital programmed cell death. Dev. Biol. *411*, 266–276.

Keenan, S.R., and Beck, C.W. (2016). *Xenopus* limb bud morphogenesis. Dev. Dyn. *245*, 233–243.

Koch, C.J. (2002). Measurement of absolute oxygen levels in cells and tissues using oxygen sensors and 2-nitroimidazole EF5. Methods Enzymol. *352*, 3–31.

Kroll, K.L., and Amaya, E. (1996). Transgenic *Xenopus* embryos from sperm nuclear transplantations reveal FGF signaling requirements during gastrulation. Development *122*, 3173–3183.

Longair, M.H., Baker, D.A., and Armstrong, J.D. (2011). Simple Neurite Tracer: open source software for reconstruction, visualization and analysis of neuronal processes. Bioinformatics *27*, 2453–2454.

Mangiavini, L., Merceron, C., Araldi, E., Khatri, R., Gerard-O'Riley, R., LeShan Wilson, T., Rankin, E.B., Giaccia, A.J., and Schipani, E. (2014). Loss of VHL in mesenchymal progenitors of the limb bud alters multiple steps of endochondral bone development. Dev. Biol. *393*, 124–136.

Martin, J.F., and Olson, E.N. (2000). Identification of a *prx1* limb enhancer. Genesis *26*, 225–229.

Montero, J.A., Lorda-Diez, C.I., Gañan, Y., Macias, D., and Hurle, J.M. (2008). Activin/TGFβ and BMP crosstalk determines digit chondrogenesis. Dev. Biol. *321*, 343–356.

Nakai, S., Watanabe, A., and Onitake, K. (1999). Sperm surface heparin/heparan sulfate is responsible for sperm binding to the uterine envelope in the newt, *Cynops pyrroghogaster*. Dev. Growth Differ. *41*, 101–107.

Ogino, H., Fisher, M., and Grainger, R.M. (2008). Convergence of a head-field selector Otx2 and Notch signaling: a mechanism for lens specification. Development *135*, 249–258.

Okada, Y.K., and Ishikawa, M. (1947). Normal table of Triturus pyrrphogaster. Jpn. J Exp. Morphol. *3*, 1–6.

Onimaru, K., Marcon, L., Musy, M., Tanaka, M., and Sharpe, J. (2016). The fin-to-limb transition as the re-organization of a Turing pattern. Nat. Commun. *7*, 1–9.

Potente, M., Gerhardt, H., and Carmeliet, P. (2011). Basic and therapeutic aspects of angiogenesis. Cell *146*, 873–887.

Provot, S., Zinyk, D., Gunes, Y., Kathri, R., Le, Q., Kronenberg, H.M., Johnson, R.S., Longaker, M.T., Giaccia, A.J., and Schipani, E. (2007). Hif-1alpha regulates differentiation of limb bud mesenchyme and joint development. J. Cell Biol. *177*, 451–464.

Puente, B.N., Kimura, W., Muralidhar, S.A., Moon, J., Amatruda, J.F., Phelps, K.L., Grinsfelder, D., Rothermel, B.A., Chen, R., Garcia, J.A., et al. (2014). The oxygen-rich postnatal environment induces cardiomyocyte cell-cycle arrest through DNA damage response. Cell *157*, 565–579.

Raspopovic, J., Marcon, L., Russo, L., and Sharpe, J. (2014). Digit patterning is controlled by a Bmp-Sox9-Wnt Turing network modulated by morphogen gradients. Science *345*, 566–570.

Ray, P.D., Huang, B.W., and Tsuji, Y. (2012). Reactive oxygen species (ROS) homeostasis and redox regulation in cellular signaling. Cell. Signal. *24*, 981–990.

Salas-Vidal, E., Lomelí, H., Castro-Obregón, S., Cuervo, R., Escalante-Alcalde, D., and Covarrubias, L. (1998). Reactive oxygen species participate in the control of mouse embryonic cell death. Exp. Cell Res. *238*, 136–147.

Salas-Vidal, E., Valencia, C., and Covarrubias, L. (2001). Differential tissue growth and patterns of cell death in mouse limb autopod morphogenesis. Dev. Dyn. *220*, 295–306.

Satoh, A., Endo, T., Abe, M., Yakushiji, N., Ohgo, S., Tamura, K., and Ide, H. (2006). Characterization of *Xenopus* digits and regenerated limbs of the froglet. Dev. Dyn. *235*, 3316–3326.

Satoh, A., Suzuki, M., Amano, T., Tamura, K., and Ide, H. (2005). Joint development in *Xenopus laevis* and induction of segmentations in regenerating froglet limb (spike). Dev. Dyn. *233*, 1444–1453.

Schmidt-Nielsen, K. (1997). Oxygen- part one. In Animal Physiology: Adaptation and Environment (Cambridge University Press), pp. 5–122.

Schnabel, D., Salas-Vidal, E., Narváez, V., Sánchez-Carbente, M., Del, R., Hernández-García, D., Cuervo, R., and Covarrubias, L. (2006). Expression and regulation of antioxidant enzymes in the developing limb support a function of ROS in interdigital cell death. Dev. Biol. *291*, 291–299.

Suda, N., Itoh, T., Nakato, R., Shirakawa, D., Bando, M., Katou, Y., Kataoka, K., Shirahige, K., Tickle, C., and Tanaka, M. (2014). Dimeric combinations of MafB, cFos and cJun control the apoptosis-survival balance in limb morphogenesis. Development *141*, 2885–2894.

Summerbell, D., Lewis, J.H., and Wolpert, L. (1973). Positional information in chick limb morphogenesis. Nature *244*, 492–496.

Suzuki, M., Satoh, A., Ide, H., and Tamura, K. (2007). Transgenic *Xenopus* with prx1 limb enhancer reveals crucial contribution of MEK/ERK and PI3K/AKT pathways in blastema formation during limb regeneration. Dev. Biol. *304*, 675–686.

Suzuki, T., Hasso, S.M., and Fallon, J.F. (2008). Unique SMAD1/5/8 activity at the phalanx-forming region determines digit identity. Proc. Natl. Acad. Sci. USA *105*, 4185–4190.

Takase, Y., Tadokoro, R., and Takahashi, Y. (2013). Low cost labeling with highlighter ink efficiently visualizes developing blood vessels in avian and mouse embryos. Develop. Growth Differ. *55*, 792–801.

Thermes, V., Grabher, C., Ristoratore, F., Bourrat, F., Choulika, A., Wittbrodt, J., and Joly, J.S. (2002). I-SceI meganuclease mediates highly efficient transgenesis in fish. Mech. Dev. *118*, 91–98.

Townsend, D.S., and Stewart, M.M. (1985). Direct development in *Eleutherodactylus coqui* (Anura: Leptodactylidae): a staging table. Copeia *1985*, 423.

Vlaskalin, T., Wong, C.J., and Tsilfidis, C. (2004). Growth and apoptosis during larval forelimb development and adult forelimb regeneration in the newt (*Notophthalmus viridescens*). Dev. Genes Evol. *214*, 423–431.

Wagenfuhr, L., Meyer, A.K., Braunschweig, L., Marrone, L., and Storch, A. (2015). Brain oxygen tension controls the expansion of outer subventricular zone-like basal progenitors in the developing mouse brain. Development *142*, 2904–2915.

Wake, D.B., and Hanken, J. (1996). Direct development in the lungless salamanders: what are the consequences for developmental biology, evolution and phylogenesis? Int. J. Dev. Biol. *40*, 859–869.

Weatherbee, S.D., Behringer, R.R., Rasweiler, J.J., IV, and Niswander, L.A. (2006). Interdigital webbing retention in bat wings illustrates genetic changes underlying amniote limb diversification. Proc. Natl. Acad. Sci. USA *103*, 15103–15107.

Yokouchi, Y., Sakiyama, J., Kameda, T., Iba, H., Suzuki, A., Ueno, N., and Kuroiwa, A. (1996). BMP-2/-4 mediate programmed cell death in chicken limb buds. Development *122*, 3725–3734.

Zelzer, E., McLean, W., Ng, Y.-S., Fukai, N., Reginato, A.M., Lovejoy, S., D'Amore, P.A., and Olsen, B.R. (2002). Skeletal defects in VEGF(120/120) mice reveal multiple roles for VEGF in skeletogenesis. Development *129*, 1893–1904.

Zou, H., and Niswander, L. (1996). Requirement for BMP signaling in interdigital apoptosis and scale formation. Science *272*, 738–741.

Zuzarte-Luis, V., and Hurle, J.M. (2005). Programmed cell death in the embryonic vertebrate limb. Semin. Cell Dev. Biol. *16*, 261–269.

Zuzarte-Luis, V., Montero, J.A., Kawakami, Y., Izpisua-Belmonte, J.C., and Hurle, J.M. (2007). Lysosomal cathepsins in embryonic programmed cell death. Dev. Biol. *301*, 205–217.

Zuzarte-Luís, V., Montero, J.A., Rodriguez-León, J., Merino, R., Rodríguez-Rey, J.C., and Hurlé, J.M. (2004). A new role for BMP5 during limb development acting through the synergic activation of Smad and MAPK pathways. Dev. Biol. *272*, 39–52.

STAR★METHODS

KEY RESOURCES TABLE

REAGENT or RESOURCE	SOURCE	IDENTIFIER
Antibodies		
Sheep Anti-Digoxigenin Fab fragments Antibody, AP Conjugated	Roche	Cat# 11093274910; RRID: AB_514497
Mouse Monoclonal Anti-Oxoguanine 8 Antibody (clone 2Q2311)	Abcam	Cat# ab64548; RRID: AB_1141628
Goat anti-mouse IgM-HRP antibody	Santa Cruz	Cat# sc-2064; RRID: AB_631776
Anti-EF5 antibody (ELK3-51 clone), Alexa 488 conjugated	Dr. Cameron J. Koch; Koch, 2002.	RRID: AB_2756854
Anti-phospho-Histone H3 (Ser10) Antibody	Millipore	Cat# 06-570; RRID: AB_310177
Goat anti-Rabbit IgG (H+L) Cross-Adsorbed Secondary Antibody, Alexa Fluor 594	Thermo Fisher Scientific	Cat# A-11012; RRID: AB_2534079
Chemicals, Peptides, and Recombinant Proteins		
Tricaine Methane Sulfonate (MS-222)	Sigma-Aldrich	Cat#A5040; CAS: 886-86-2
Proteinase K	Roche	Cat#RPROTK-RO
Blocking reagent	Roche	Cat#11096176001
Dig RNA labeling mix	Roche	Cat#11277073910
LysoTracker green, DND-26	Thermo Fisher Scientific	Cat#L7526
LysoTracker red, DND-99	Thermo Fisher Scientific	Cat#L7528
Dihydroethidium	Sigma-Aldrich	Cat#7008; CAS: 104821-25-2
CellROX Deep Red	Life Technologies	Cat# C10422
Diaminobenzidine (DAB)	Sigma	Cat# D4293; CAS: 91-95-2
Mesenchymal Stem Cell medium	ScienCell Research Laboratories	Cat#7501
N-acetyl-cysteine (NAC)	Sigma-Aldrich	Cat#7250; CAS: 616-91-1
EF5 nitroimidazole	Dr. Cameron J. Koch	CAS: 152721-37-4
Hoechst 33342, Trihydrochloride, Trihydrate - 10-mg/mL Solution in Water	Invitrogen	Cat#H3579; CAS: 23491-52-3
VECTASHIELD Antifade Mounting Medium	Vector Laboratories	Cat#H-1000
VECTASHIELD Antifade Mounting Medium with DAPI	Vector Laboratories	Cat#H-1200
Critical Commercial Assays		
RNeasy Mini kit	Qiagen	Cat#74104
T7 RNA polymerase	Promega	Cat#P2075
SP6 RNA polymerase	Promega	Cat#P1085
In-Fusion HD Cloning Kit	Clontech	Cat# 639648
Experimental Models: Organisms/Strains		
Wild-type chicken eggs		N/A
Wild-type *X. laevis* tadpoles	Dr. Haruki Ochi	N/A
Wild-type Japanese fire-bellied newts	Dr. Akihiro Watanabe	N/A
Wild-type coqui frogs	Dr. James Hanken	N/A
X. laevis: *Prrx1-VegfA-EGFP*	This paper	N/A
Oligonucleotides		
Forward primers for *X. laevis bmp4a* RNA probes: GAGCCAGTTCCTTAGTATCATC	This paper	N/A
Reverse primers for *X. laevis bmp4a* RNA probes: GCAAATAAATAGGGAGGATCTG	This paper	N/A
Forward primers for *X. laevis msx2* RNA probes: TTGAAACCTCATCGGTCAAGTCGG	This paper	N/A

(*Continued on next page*)

Continued

REAGENT or RESOURCE	SOURCE	IDENTIFIER
Reverse primers for *X. laevis msx2* RNA probes: GCAGTAGTAAGTCCTGTACAGCTG	This paper	N/A
Forward primers for *X. laevis VegfA* ORF with *HindIII* and Kozak sequences: GGCGAGTTCTAGCTGAAGC TTGCC ACCATGAACTTTCTGCCGAGCTG	This paper	N/A
Reverse primers for *X. laevis VegfA* ORF with *ClaI* and *EcoRI* sequences: GCGACCGGAATTCGAATCG ATTTCCGTCGTG GCTTTTCACATC	This paper	N/A
Forward primers for mouse *Prrx1* promoter with *KpnI* sequence: CTATAGGGCGAATTGGGTACCTTG CTACA GCTTTCTAGAACAATG	Suzuki et al., 2007; this paper	N/A
Reverse primers for mouse *Prrx1* promoter with *HindIII* sequence: AAAGTTCATGGTGGCAAGCTTAATAG GAG CCTGTAATTACGTG	Suzuki et al., 2007; this paper	N/A
Recombinant DNA		
pGEM-T Easy plasmid	Promega	Cat#A1360
ISXexEGFP plasmid	National Bio-resource Project of the Japan (NBRP) *X. tropicalis*	N/A
EF1α-VegfA-EGFP plasmid	This paper	N/A
Prrx1-VegfA-EGFP plasmid	This paper	N/A
X. laevis bmp4a/ pGEM-T Easy plasmid for probe synthesis	This paper	N/A
X. laevis msx2/ pGEM-T Easy plasmid for probe synthesis	This paper	N/A
Software and Algorithms		
Fiji	ImageJ	https://fiji.sc/
Cell counter plug in	ImageJ	https://imagej.nih.gov/ij/plugins/cell-counter.html
GraphPad 8.0.2	Prism	N/A
Photoshop CS6	Adobe	N/A
Zen Black lite	Zeiss Microsystems	https://www.zeiss.com/microscopy/int/downloads/zen.html
Other		
Multigas incubator	Astec	Cat# APM-30D
Regular incubator	Fukushima	Cat# FMU-053
Dissolved oxygen meter	Satotech	Cat# DO-5509

CONTACT FOR REAGENT AND RESOURCE SHARING

Further information and requests for resources and reagents should be directed to and will be fulfilled by the Lead Contact, Mikiko Tanaka (mitanaka@bio.titech.ac.jp).

EXPERIMENTAL MODEL AND SUBJECT DETAILS

All animal experiments were performed in accordance with guidelines for animal experiments of Tokyo Institute of Technology, Yamagata University, and Harvard University, and the experimental protocols were approved by the committees of Tokyo Institute of Technology, Yamagata University, and Harvard University. Fertilized chicken (*Gallus gallus*) eggs were incubated at 37.5°C in a humidified incubator until the desired Hamburger-Hamilton (HH) stage (Hamburger and Hamilton, 1951). African clawed frog (*Xenopus laevis*) tadpoles were kept in 0.1% sea-salt solution and staged according to a developmental table (Gurdon, 1995). Japanese fire-bellied newt (*Cynops pyrrhogaster*) larvae were kindly provided (Nakai et al., 1999) by Dr. Akihiko Watanabe (Yamagata University), kept in filtered water and staged (Okada and Ishikawa, 1947). Coquí frog (*Eleutherodactylus coqui*) eggs were kept in 10% Holtfreter solution (Hanken et al., 2001) and staged according to Townsend-Stewart (TS) stages (Townsend and Stewart, 1985). Tadpoles or larvae were anaesthetized with 0.25 mg/ml Tricaine Methane Sulfonate (Sigma-Aldrich) prior to experimental manipulations.

METHOD DETAILS

Probe Synthesis and In Situ Hybridization

Total RNA was extracted from *X. laevis* or chicken embryos using the RNeasy kit (Qiagen). cDNA was synthesized by reverse transcription and used as a template for PCR. To isolate gene fragments, we used primers based on sequences of *X. laevis bmp4a* (GenBank: NM_001088032) and *X. laevis msx2* (Ensembl: ENSXETT00000020130). Gene fragments were cloned into pGEM-Teasy vectors (Promega) and transcribed using T7 (Promega) (*X. laevis bmp4*) or SP6 (Promega) (*X. laevis msx2*) RNA polymerases. Whole-mount in situ hybridization was performed as described previously (Satoh et al., 2006).

Detection of Cell Death and Reactive Oxygen Species

Cell death was detected using 0.5 μM Lysotracker Red or Green (Thermo Fisher Scientific, Waltham, MA) in PBS+ (PBS pH 7.4, 9 mM $CaCl_2$,3.3 mM $MgCl_2$) or under the same conditions described below for DHE. Reactive oxygen species generation was detected in non-fixed whole tadpoles or isolated chicken limbs using dihydroethidium (DHE, Sigma-Aldrich) or CellROX Deep Red (Life Technologies). Tadpoles were incubated with DHE 8 μM in PBS pH 6.5 for 1 hr at 25°C, and chicken for 2 hr at 37°C, washed with PBS and observed immediately. Alternatively, tadpoles were incubated with 5 μM CellROX Deep Red (Life Technologies) in PBS+ for 1 hr at 25°C, fixed with 4% paraformaldehyde for 15 min and mounted with Vectashield (Vector Laboratories).

Immunohistochemistry

Chicken limbs were fixed overnight with 4% paraformaldehyde/PBS and *X. laevis* limbs were fixed for 3 hr with MEMFA (100 mM MOPS pH 7.4, 2 mM EGTA, 1 mM $MgSO_4$, 3.7% formaldehyde). Samples were then incubated with sucrose 30% overnight, embedded in OCT compound (Tissue-Tek, Sakura Finetek), frozen with liquid nitrogen and sectioned at 10 μm using a cryostat (CM3050 S, Leica). Endogenous peroxidases were blocked with 3% H_2O_2/PBS for 20 min and antigen retrieved with 0.3% Triton X-100/PBS for 1 hr. After blocking with 1% BSA/0.3% Triton X-100/PBS, sections were incubated overnight at 4°C with 1:100 anti-8-oxoguanine antibody (ab 64548, Abcam). Sections were washed with PBS and incubated overnight with 1:250 anti-mouse IgM/HRP antibody (sc-2064, Santa Cruz). After washing, color was developed with 100 μg/ml DAB (Sigma)/0.03% H_2O_2/PBS and sections were mounted using Vectashield containing DAPI (Vector Laboratories).

Cell Proliferation Analysis

Proliferation was detected using the mitosis marker anti-phospho-histone H3 as described before (Suzuki et al., 2007), with minor modifications. Embryos were fixed overnight with 4% paraformaldehyde/PBS, incubated with sucrose 30% for at least 3 h, embedded in OCT, frozen in liquid nitrogen and sectioned at 10 μm. Slides were washed with PBT buffer (0.02% Tween 20/PBS), blocked with 1% normal goat serum/ 0.1% Triton X-100/ 0.02% Tween 20/PBS and incubated with 1:500 rabbit anti-phospho-histone H3 (06-570, Millipore) in blocking solution overnight at 4°C. After washing with PBT, slides were incubated with 1:500 goat anti-rabbit Alexa Fluor-594 conjugated antibodies (06-570, Millipore) in blocking solution for 2 hr at room temperature and then washed again. Nuclear counterstaining was performed with Hoechst 33342 solution (H3570, Invitrogen) 1:1000 in PBS for 10 min. After washing with PBS, slides were mounted with Vectashield.

Visualization of Blood Vessels

Blood vessels were visualized through intravascular injection of purple highlighter ink diluted 1:1 in PBS (PUSR80.12 cartridge, Mitsubishi Pencil) using pulled glass capillaries (Narishige) and an aspirator tube assembly (Drummond Scientific Company) (Takase et al., 2013). Ink was injected in the chicken's chorioallantoic membrane or any major blood vessel of anaesthetized tadpoles or larvae. After 10 min, samples were fixed with 4% paraformaldehyde for at least 3 hr and photographed.

Oxygen or NAC Incubation

Incubations under low (5%) or high (65%) oxygen atmosphere were made using a multigas incubator (APM-30D, Astec). Normoxic controls were incubated at atmospheric oxygen levels using a regular incubator (FMU-053, Fukushima Industries). Oxygen levels in the water were measured using a dissolved oxygen meter (DO-5509, Satotech). Isolated chicken limbs were incubated in 400 μL Mesenchymal Stem Cell medium (ScienCell Research Laboratories) for 6 hr in 24-well plates. Tadpoles were incubated immersed in 1.8 cm depth 0.1% sea-salt solution at 25°C, either individually in 6-well plates for 3 hr or in 90 mm Petri dishes for 1 week. N-acetyl-cysteine (Sigma) was dissolved in PBS and used at 1 mg/L.

Plasmid Construction and Generation of *X. laevis* Transgenics

For constructing the plasmids, the open reading frame of *X. laevis VegfA* (GenBank: NM_001097785.1) was amplified by PCR from stage 27 *X. laevis* cDNA using primers that included *Hind* III and Kozak sequences at the N terminus and *Cla*I and *EcoR*I sequences at the C terminus. The resulting PCR product was then cloned into the *ISXexEGFP* plasmid (Thermes et al., 2002) into *Hind* III and *Cla*I sites via In-Fusion reaction (Clontech), resulting in the *EF1α-VegfA-EGFP* plasmid. The mouse *Prrx1* promoter, which drives limb-specific expression in *X. laevis* tadpoles (Suzuki et al., 2007), was amplified by PCR from mouse genomic DNA using primers that included *Kpn*I sequence at the N terminus and *Hind* III sequence at the C terminus. The resulting PCR product was then cloned into *Kpn*I and *Hind* III sites via In-Fusion reaction, forming the *Prrx1-VegfA-EGFP* plasmid. Transgenic *X. laevis* embryos

were generated by injecting an unfertilized egg with 150 ng of *Prrx1-VefgA-EGFP* plasmids, sperm nucleus and oocyte extract (Kroll and Amaya, 1996; Ogino et al., 2008).

Quantitative Measurement of Oxygen Tension in the Tissue

Oxygen levels were measured using EF5 compound and ELK3 Alexa Fluor 488 conjugated antibodies provided by Dr. Cameron J. Koch. EF5 is reduced under hypoxia, forming adducts with cysteine residues of proteins which are recognized by ELK3 antibodies conjugated to a fluorescent dye (Koch, 2002). 100 of EF5 solution (10 mM EF5, 9 mg/ml NaCl) was pipetted over the chicken embryo, which was then incubated for 3 hr at 37 °C. Alternatively, X. laevis tadpoles were kept in Petri dishes with 100 μM EF5 in 0.1% sea-salt solution for 3 hr. Limbs were then fixed for 3 hr with PFA 4%, cryoprotected with sucrose 30%, mounted in OCT and sectioned at 12 μm. After blocking overnight, immunostaining was performed for 6 hr using regular ELK3-488 antibodies at 75μg/ml or competed ELK3-488 antibodies (75 μg/ml ELK3-488 mixed with 0.5 mM EF5) as a control (Koch, 2002).

Images

Images were captured using the LSM780 confocal microscope (Zeiss), TCS SPE confocal microscope (Leica) or stereomicroscope (MZ16F, Leica). Collage of multiple panels was made using Photoshop CS6 (Adobe) software. Pseudocolor images were generated using Zen black software (Zeiss).

The following panels were flipped horizontally: Figures 1B, 1F, 1F', 1R, 2D, 2E, 2 (G–I)', 2K, 2L, 3B, 3B', 3F, S1A (stage 55), S1B (early stage 54), S1C (stage 53), S1D (stages 55 and 56), S1E (early stage 54), S3D, S3I, S3J, S4D, S5A (HH27), S5B (stages 53 and 55), S6C, S7B, S7F, S7F', S7H and S7H'.

The following panels are collages of multiple images: Figures 1A, 1E, 1H, 2A (HH31), 2H, 2I, 3D, 3E, S1D (early stage 54, stage 55 and 56), S1E (early stage 54, stage 55 and 56), S2E–S2H, S3E, S3F, S5A (HH31, HH33 and HH35), S5E and S7M.

The following panels are epifluorescence images: Figures 3C, 3F, S3D, S3E, S4A–S4B', S2I, S5C, S5E, S6D and S6E.

The following panels are confocal images: Figures 1A, 1E, 1E', 1I–1K, 4A, 4A', 4C, 4C', 4E, 4F', 4H, 4I', S2A–S2H, S7B–S7H', and S7K–S7N.

The following panels are maximum intensity projections of confocal image stacks including the whole interdigital region: Figures 1B, 1F, 1F', 1M, 1N, 1P, 1Q, 2A–2E, 2 (G–I)', 2K, 2L, 3A–3E, S1D–S1F, S3A–S3C, S4C, S4D, S5A, S5B, S5D, S5G and S6A–S6C.

QUANTIFICATION AND STATISTICAL ANALYSIS

Quantification

Quantification of cell death was done by manually counting cells in the interdigital region using fiji Cell Counter plugin. Cell proliferation was shown as number of pH3-positive cells divided by area (μm^2) × 10^4. The area of the digits or interdigits was measured using Fiji.

For quantification of the blood vessel density, the blood vessel paths were manually traced using the fiji Simple Neurite Tracer plug in (Longair et al., 2011) and represented as blood vessel distance in μm.

Intensity of EF5-ELK3 fluorescence was measured using fiji. Background fluorescence was subtracted from each measurement.

Measurement of the amount of interdigital webbing – or limb sinuosity – was performed as described (Jaekel and Wake, 2007). The outline of the limb between digits 1 and 5 was measured and divided by the linear distance between these two points, yielding the limb sinuosity.

Statistical analysis

All statistical analyses were done with Prism 8.0.2 (GraphPad). *n* numbers are biological repeats and measurements are represented as mean ± SEM. Significance was determined using two-tailed paired t-tests for comparison between control (left) and experimental (right) sides, two-tailed unpaired t-tests for comparison between limbs of different animals or two-way ANOVA with Tukey's multiple comparisons test for analyzing two factors (measurement of oxygen tension under experimental conditions only). Statistical details can be found in the legends. Significance was defined as $P \leq 0.05$ (*$p < 0.05$, **$p < 0.01$, ***$p < 0.001$).